

Novel phases in the Fe-Si-O system at terapascal pressures

Nan Huang¹, Renata M. Wentzcovitch^{2,3,4,5,†}, Zepeng Wu¹, Feng Zheng⁶, Bingxin
Wu¹, Yang Sun^{1,‡}, Shunqing Wu^{1,*}

¹*Department of Physics, OSED, Key Laboratory of Low Dimensional Condensed Matter Physics (Department of Education of Fujian Province), Xiamen University, Xiamen 361005, China*

²*Department of Applied Physics and Applied Mathematics, Columbia University, New York, NY 10027, USA*

³*Department of Earth and Environmental Sciences, Columbia University, New York, NY 10027, USA*

⁴*Lamont-Doherty Earth Observatory, Columbia University, Palisades, NY 10964, USA*

⁵*Data Science Institute, Columbia University, New York, NY 10027, USA*

⁶*School of Science, Jimei University, Xiamen, 361021, China*

Abstract

The Fe-Si-O ternary system, central to modeling the interiors of terrestrial planets, remains poorly constrained at Terapascal (TPa) pressures characteristic of super-Earth mantles. Using a combination of crystal-structure prediction and *ab initio* calculations, we identify three ternary compounds stable near 1 TPa: $P3$ FeSiO_4 , $P3$ $\text{Fe}_4\text{Si}_5\text{O}_{18}$, and $\bar{P3}$ FeSi_2O_6 . The first two phases are thermodynamically stable at low temperatures, whereas $\bar{P3}$ FeSi_2O_6 becomes favored above ~ 2000 K. All three are metallic, paramagnetic, and adopt pseudo-binary arrangements derived from the FeO_2 and SiO_2 end-member structures. Their crystal structures emerge through substitutions of Fe for Si in Fe_2P -type SiO_2 or of Si for Fe in $Pnma$ -type FeO_2 , the stable elemental oxides at ~ 1 TPa. This structural continuity suggests that Fe preferentially substitutes for Si in the canonical Mg-silicates expected at TPa pressures. Notably, these new pseudo-binaries accommodate Fe in six- and nine-fold coordination, in contrast to the eight-fold cubic coordination found in FeO at similar pressures. The thermodynamic conditions under which these phases form from FeO_2 and SiO_2 mixtures are clarified through quasi-harmonic free-energy calculations. Their prevalence in super-Earth mantles is found to depend on the abundance of FeO_2 , which in Earth's deep mantle may be generated by the dehydrogenation of FeOOH goethite. The existence of these phases implies a markedly different pattern of Fe incorporation into high-pressure Mg-silicates at TPa conditions, compared with the behavior inferred at the GPa pressures of Earth's mantle.

[†]Email: rmw2150@columbia.edu

[‡]Email: yangsun@xmu.edu.cn

^{*}Email: wsq@xmu.edu.cn

1. Introduction

Ab initio materials simulations at extreme pressures and temperatures have reached a level of maturity that enables robust predictions of the physical properties of complex mineral assemblages and melts under conditions typical of planetary interiors, e.g., up to \sim 6,500 K and 3.6 Mbar in Earth and beyond (e.g., [1]). Earth remains the most comprehensively studied planet and the only one known to support life. Investigations of mantle-forming phases and their properties have provided critical insights into seismological observations, informing models of Earth's internal structure and dynamics.

The methodologies developed through these studies are now being extended to investigate other solar and extrasolar terrestrial materials, particularly those of super-Earth-type planets with masses of up to \sim 14 M \oplus . These planets are being rapidly discovered and are of high interest due to their potential habitability. Comparative planetology, specifically the study of planetary interior structure, evolution, and dynamics, requires characterizing planet-forming phases under the extreme conditions expected in these bodies, which may reach temperatures of up to \sim 10,000 K and pressures of up to 3 TPa in terrestrial planets with masses of up to \sim 20 M \oplus [2-4].

In the past two decades, the discovery of novel high-pressure phases has accelerated following the identification of the MgSiO₃ post-perovskite phase in 2004 [5-7], the highest-pressure Mg-silicate known in Earth's mantle. Coincidentally, the detection of the super-Earth 55 Cancri-e [8] around the same time sparked interest in the Mg-Si-O system at high pressures, the dominant chemical system in rocky planetary mantles. All major computationally discovered phases in the Mg-Si-O system, up to 3 TPa [1,9-14], have also been predicted in low-pressure analogs, such as NaMgF₃ and MgGeO₃ [15,16] and subsequently confirmed experimentally [17-19]. Notably, high-pressure phases often exhibit cation disorder [16,19,20].

Despite this progress, one of the major remaining challenges is the incorporation of iron, an abundant and geophysical critical element, into these high-pressure systems. In Earth's lower mantle, iron exists primarily as Fe²⁺ or Fe³⁺, substituting for Mg and/or

Si. In this work, we initiate the extension of the Mg-Si-O system to include iron by exploring the stable Fe-Si-O ternary phases as possible end members at ~ 1 TPa. This investigation builds on the extensive prior studies of the relevant binary systems, Fe-O [21,22] and Si-O [12-15] systems at high pressures.

The following section describes the computational methods employed, including structure prediction using the adaptive genetic algorithm (AGA) [23]. Section 3 presents and discusses the discovered high-pressure phases, assessing their thermodynamic stability at elevated temperatures. We conclude this study by summarizing our findings in Section 4.

2. Computational methods

First-principles calculations were performed using the finite-temperature version of density functional theory (DFT) [24,25], as implemented in the Quantum ESPRESSO (QE) package [26,27]. The exchange-correlation functional was treated using the non-spin-polarized local density approximation (LDA). Spin-polarized calculations were performed for the low-energy phases, but the magnetic moments were found to be quenched in self-consistent calculations. Vanderbilt-type ultrasoft pseudopotentials [28] were employed for Fe, Si, and O, with the valence electronic configuration of $3s^23p^63d^{6.5}4s^1$ (Fe), $3s^23p^1$ (Si), and $2s^22p^4$ (O). These potentials were previously tested and used in a few studies at TPa pressures [22,29]. A kinetic energy cutoff of 50 Ry and a charge density cutoff of 500 Ry were applied. Brillouin-zone integration was performed over a Monkhorst-Pack k-point grid of $2\pi \times 0.03 \text{ \AA}^{-1}$ in the structure optimization. Structural optimization was performed under constant pressure using the Broyden-Fletcher Goldfarb-Shanno (BFGS) algorithm [30-33] with variable cell shape. The convergence thresholds are 0.01 eV/ \AA for the atomic force, 0.05 GPa for stress tensor components, and 1×10^{-5} eV for the total energy.

The finite displacement method was used to compute phonon frequencies. Supercells for phonon calculations were ($4 \times 4 \times 3$) for $P3$ FeSiO_4 , ($2 \times 2 \times 2$) for $P3$ $\text{Fe}_4\text{Si}_5\text{O}_{18}$, and ($2 \times 2 \times 4$) for $P\bar{3}$ FeSi_2O_6 , with a uniform Monkhorst-Pack k-point mesh of density 2π

$\times 0.03 \text{ \AA}^{-1}$. The second-order force constants and harmonic phonon dispersion curves were obtained using the PHONOPY code [34]. The thermodynamic properties at finite temperatures were investigated within the quasi-harmonic approximation (QHA) [35,36] and the qha code [37]. Although the electronic entropy affects phonons, we used the electronic entropy at 4000 K to approximate the contributions at all temperatures.

For crystal structure prediction using the AGA [23] assisted by classical auxiliary embedded-atom method (EAM) potentials [38] was employed. In EAM, the total energy of an N -atom system was evaluated by

$$E_{\text{total}} = \frac{1}{2} \sum_{i,j(i \neq j)}^N \phi(r_{ij}) + \sum_i F_i(n_i), \quad (1)$$

where $\phi(r_{ij})$ denotes the pair repulsion between atoms i and j with a distance of r_{ij} ; $F_i(n_i)$ is the embedded term with the electron density term $n_i = \sum_{j \neq i} \rho_j(r_{ij})$ at the site occupied by atom i . The fitting parameters in the EAM formula were chosen as follows: The pair interactions were modeled by the Morse function,

$$\phi(r_{ij}) = D \left[e^{-2\alpha(r_{ij}-r_0)} - 2e^{-\alpha(r_{ij}-r_0)} \right], \quad (2)$$

where D , α and r_0 are fitting parameters. The density function is modeled by an exponentially decaying function,

$$\rho(r_{ij}) = \alpha \exp[-\beta(r_{ij} - r_0)], \quad (3)$$

where α and β are fitting parameters. The form proposed by Banerjee and Smith in Ref. [39] was used as the embedding function with fitting parameters F_0 , γ as

$$F(n) = F_0[1 - \gamma \ln n]n^\gamma. \quad (4)$$

The potential fitting was performed using the force-matching method with a stochastic simulated annealing algorithm as implemented in the POTFIT code [40,41].

3. Results and discussion

3.1 Survey of relevant binary systems

The phase transitions of the elemental and binary phases of the Fe-Si-O system have been extensively studied in previous works. We first review the ground-state structures of the most stable binaries SiO_2 [12-14], FeO_2 , Fe_2O , and FeO [21,22] within the 0.5–1.3 TPa pressure range (see Figure. 1(a)). Their crystal structures are shown in Figure. 1(b) and (c), where the high-temperature phase Cotunnite-type SiO_2 is also included. The pyrite-type phase ($Pa\bar{3}$) of SiO_2 transitions to the $R\bar{3}$ phase at 667 GPa, which then transitions to the Fe_2P -type structure above 914 GPa. FeO_2 transitions from $R\bar{3}m$ symmetry to the orthorhombic $Pnma$ structure at 562 GPa, and this $Pnma$ phase remains stable up to 1.3 TPa. Fe_2O retains its $I4/mmm$ structure throughout the entire pressure range. FeO transitions from the $R\bar{3}$ phase to $Cmcm$ symmetry at ~570 GPa, and then to the B2 (CsCl-type) structure above 835 GPa. These phase transitions are consistent with the work of others [12-14,21,22], although minor discrepancies in transition pressures may stem from differences in computational methods.

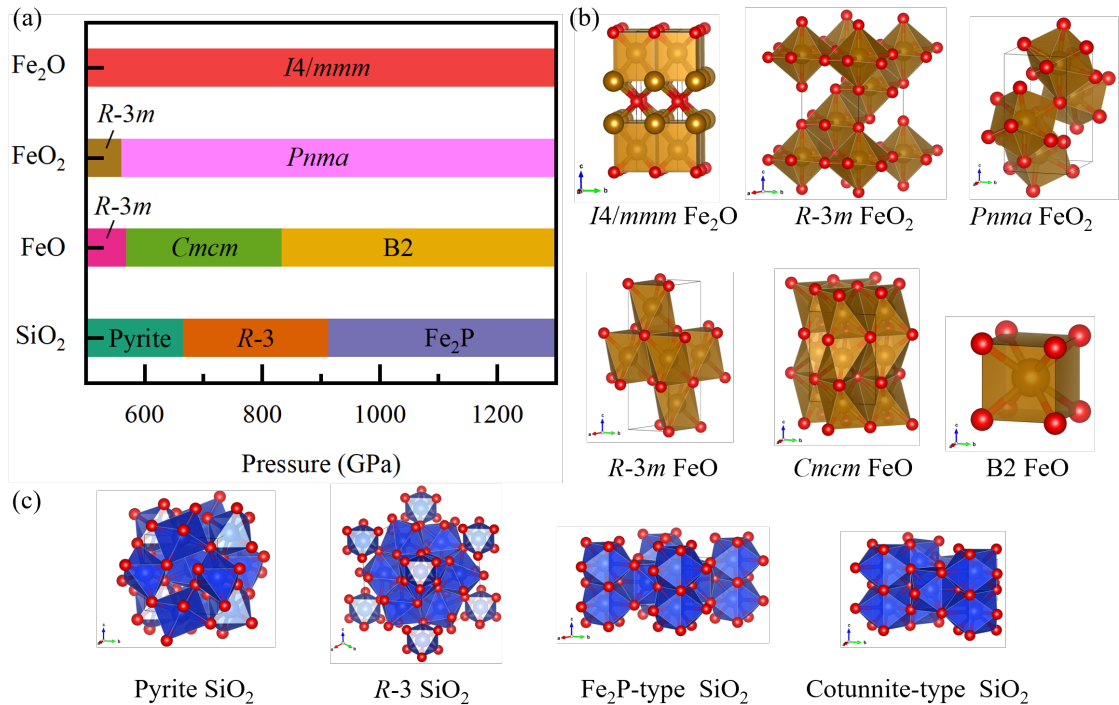


Figure 1. (a) Phase relations in SiO_2 , FeO_2 , Fe_2O , and FeO within the 0.5–1.3 TPa pressure range. Crystal structures of (b) Fe-O binaries and (c) SiO_2 mentioned in (a). The Cotunnite-type in (c) is a high-temperature version Fe_2P -type SiO_2 .

3.2 Crystal structure prediction

Using our AGA crystal structure prediction method [23], we performed successive structural searches for the Fe-Si-O system at 1 TPa. We systematically explored the compositional space of the Fe-Si-O system by selecting distinct components characterized by the formula $\text{Fe}_x\text{Si}_y\text{O}_z$. The parameters x, y, and z are integers constrained to the set $\{(x,y,z) \mid x,y,z \in \{1,2,3,4\} \text{ and } x+y+z \leq 10\}$. Each combination was reduced to its simplest form and used from 1 to a maximum of 10 formula units and not more than 30 atoms per cell for the search. We have also explored prospective pseudo-binaries of the Fe-Si-O system. By selecting multiple pairs of edge end members in the convex hull, we have conducted searches by combining them in the ratios of 1:1, 1:2, 1:3, 2:1, and 3:1, respectively.

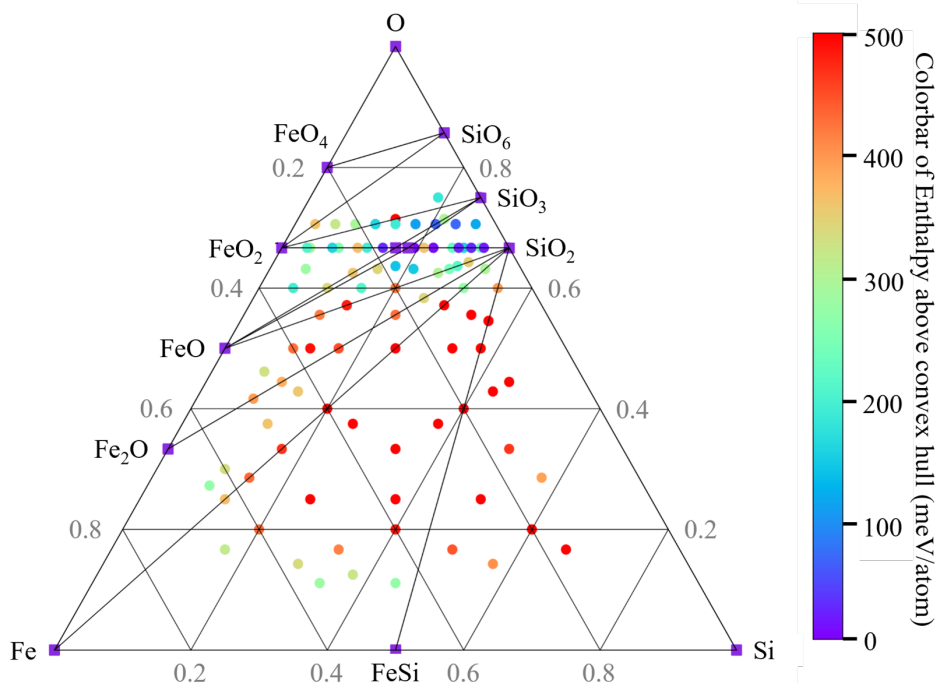


Figure 2. Convex hull of the Fe-Si-O system at 1 TPa and 0 K. Purple squares indicate endmembers and compounds on the convex hull, and solid circles represent the compositions searched in this study. The color gradient from purple to red signifies an increasing magnitude of H_d (formation enthalpy distance above the convex hull).

After a series of searches to locate energetically favorable stoichiometries, refining the search, and performing configuration substitutions, three stable phases were

identified: $P3$ FeSiO_4 , $P3$ $\text{Fe}_4\text{Si}_5\text{O}_{18}$, and $P\bar{3}$ FeSi_2O_6 , among which only $P\bar{3}$ FeSi_2O_6 exhibited thermodynamic stability at high temperatures. Phonon dispersions for the three structures are depicted in Figure. S2. The absence of imaginary vibrational frequencies indicates good dynamical stability of these phases. Figure. S2 also presents their band structures and the projected electronic density of states. It shows that all three structures are metallic at 1 TPa, with the electronic density of states dominated by oxygen and iron states.

Figure. 2 illustrates the convex hull at 1 TPa and 0 K, where phases with formation enthalpies (ΔH) below the convex hull are thermodynamically stable. The stability hierarchy is quantified by the distance to the convex hull, H_d , where $H_d = 0$ corresponds to the ground state.

3.3 Structural analysis

The crystal structures of $P3$ FeSiO_4 , $P3$ $\text{Fe}_4\text{Si}_5\text{O}_{18}$, and $P\bar{3}$ FeSi_2O_6 are shown in Figure. 3(a), and their crystallographic data are shown in Table S1. These crystalline phases exhibit a high degree of structural similarity. They bear a marked resemblance to the Fe_2P -type SiO_2 , possessing similar Si-O polyhedra. The non-oxygen ions within the ab -plane have identical arrangements. Notably, Fe in $P3$ FeSiO_4 and $P3$ $\text{Fe}_4\text{Si}_5\text{O}_{18}$ exhibit two distinct coordination environments: six-fold and nine-fold. In contrast, only six-fold coordinated Fe ions are found in the $P\bar{3}$ FeSi_2O_6 phase. 6-fold ions are configured in an octahedral geometry, while the nine-fold sites form tri-capped trigonal prisms (XO_6) augmented by three additional oxygen ions (XO_{6+3}) positioned outside the centers of the rectangular faces, as indicated by the white and black lines in Figure. 3(b). The oxygen sublattice in the three structures, as well as in Fe_2P -type SiO_2 , is composed of distorted hexagonal layers that are stacked along the c axis and exhibit relative slip (displacement) between adjacent layers parallel to the ab -plane. Considering the oxygen sublattice as the primary framework, all these structures can be conceptualized as resulting from the filling of interstitial sites within the oxygen sublattice. The nine-fold silicon or iron co-plane with the oxygen layers, whereas the

six-fold iron intercalates between these oxygen layers. Let the height of a single tri-capped prism in the c -direction be denoted as d . Polyhedra with the same coordination stack along the c -axis. The tri-capped prisms are connected via sharing their apical (or basal) faces. Adjacent columns exhibit a relative displacement of $d/2$ along the c -axis; correspondingly, two octahedra within the same column are also separated by a distance of d . Oxygens are exclusively four-fold coordinated with iron or silicon, forming tetrahedral structures. Only two distinct coordination motifs are observed in these tetrahedra: O-Fe₂Si₂ and O-FeSi₃.

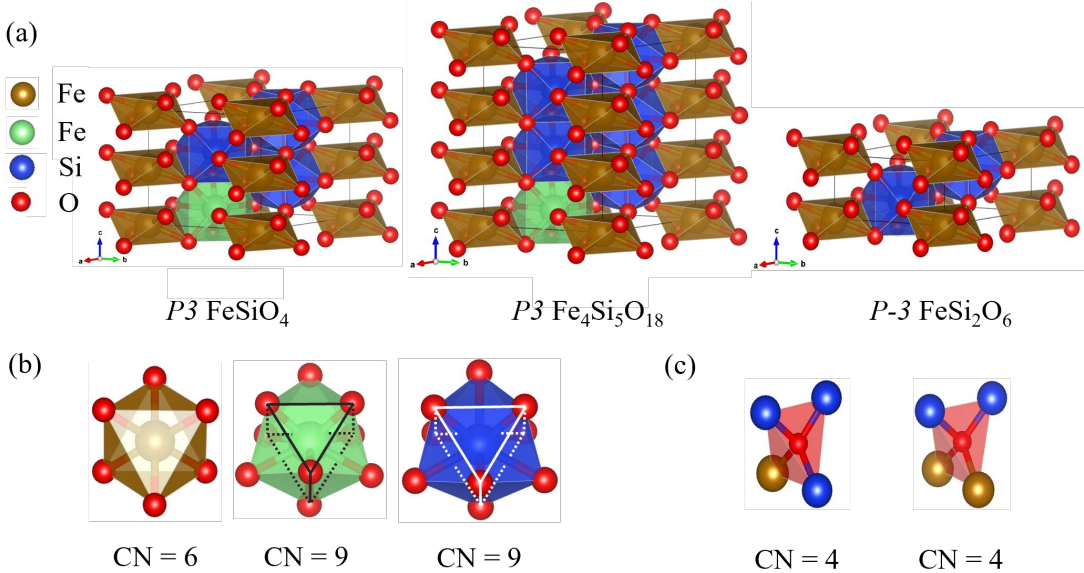


Figure 3. Structural details of novel Fe-Si-O ternary phases. (a) Crystal structures of $P3$ FeSiO₄ (left), $P3$ Fe₄Si₅O₁₈ (middle), and $P\bar{3}$ FeSi₂O₆ (right). Atoms are represented by spheres of different colors: brown for iron (Fe), blue for silicon (Si), and red for oxygen (O). (b) Three polyhedral types, i.e., FeO₆ (brown), FeO₉ (green), and SiO₉ (blue) exist in these structures. The white and black lines indicate the trigonal prisms centered on non-oxygen ions. (c) Polyhedra centered on oxygens are four-fold coordinated and form tetrahedra.

Structural comparison reveals a series of analogous compounds to these novel Fe-Si-O ternary phases, namely NaLnF₄ (where Ln = La, Ce, Pr, Nd, Sm, or Gd) [42,43]. These compounds exhibit intrinsic disorder, with the six-fold coordinated sites occupied by Na, while the nine-fold coordinated sites are occupied by a mixture of Na and Ln. Another series of halides has also been found to possess structures similar to

our newly discovered structures [44]. The existence of these low-pressure analogs allows for an effective study of the properties and structural evolution of the Fe-Si-O high-pressure system under laboratory conditions, i.e., whether dissociation into binary occurs under pressure and what the binary structures would be, similar to the low-pressure analogs of MgSiO_3 , namely, NaMgF_3 and MgGeO_3 [15,16].

It is noted that $P3$ FeSiO_4 and $P3$ $\text{Fe}_4\text{Si}_5\text{O}_{18}$ can be derived through stacking of $P-3$ FeSi_2O_6 units and atomic Si-Fe replacements (see Figure. 3(a)). Consequently, it is reasonable to regard $P\bar{3}$ FeSi_2O_6 is the basic unit for this category of pseudo-binaries. Here, we aim to elucidate the structural relationship between $P\bar{3}$ FeSi_2O_6 and the structure of the endmembers of this pseudo-binary system, i.e., Fe_2P -type SiO_2 and $Pnma$ -type FeO_2 (see Figure. 4(a)).

Starting from the structure of SiO_2 at 1 TPa, we investigate the type of structure obtained when Si is replaced by Fe, i.e., starting with the Fe_2P -type FeO_2 . Upon structural optimization, the structure maintains $P\bar{6}2m$ symmetry. Phonon calculations produce imaginary frequencies, indicating structural instability in Fe_2P -type FeO_2 . Structural relaxation with an added eigenmode of the most unstable mode at the Gamma-point of the Brillouin Zone produces a $P31m$ -type FeO_2 structure. The latter results from significant Fe displacement from the higher-symmetry site and produces a six-fold coordinated Fe (see Figure. 4(c)). Retaining one FeO_6 unit and replacing the two remaining Fe with Si yielded $P\bar{3}$ FeSi_2O_6 upon structural optimization, showing the Si's preference for nine-fold coordination. In short, simple substitution of Si by iron in Fe_2P -type SiO_2 produces distortions and displacements leading to $P\bar{3}$ FeSi_2O_6 .

Similarly, we created $Pnma$ SiO_2 in the same configuration as the ground state of FeO_2 at 1 TPa, and optimized the structure. As a result, we obtained the high-temperature cotunnite-type phase of SiO_2 at 1 TPa, which is very similar to Fe_2P -type SiO_2 , the low-temperature polymorph. The primitive cell of cotunnite-type SiO_2 is orthorhombic and contains 12 atoms, whereas that of $P\bar{3}$ FeSi_2O_6 is trigonal and

contains 9 atoms. To see more easily the relationship between the cotunnite and the $P\bar{3}$ structures it is necessary to first construct supercells capable of accommodating both structures. To this end, a three-fold SiO_2 supercell corresponding to a four-fold orthorhombic FeSi_2O_6 supercell was constructed, as illustrated in Figure. 4(b). Then, we substituted the corresponding atoms in $Pnma$ SiO_2 with the same arrangement of Fe and Si as in FeSi_2O_6 . After relaxation, we obtained a $Pnma$ FeSi_2O_6 structure.

To achieve a Si-O framework identical to that of the $P\bar{3}$ phase, additional displacements along the c -axis are required for the Si atoms marked in green in Figure. 4(a). They are the same displacements that transform the cotunnite structure of SiO_2 to the Fe_2P -type structure [12], i.e., displacement of some Si ions along the c -axis. We fixed the c -coordinates of the non-green cations in $Pnma$ FeSi_2O_6 and employed the Nudged Elastic Band (NEB) method [45] to calculate the energy barrier for the transition from $Pnma$ to the $P2_1/m$ phase (with a Si-O sublattices consistent with that of $P\bar{3}$). As shown in Figure. 4(d), the energy barrier was found to be 0.32 eV/atom, corresponding to a temperature of ~ 3700 K. This produced a structure with $P2_1/m$ symmetry. The energy difference between these structures is ~ 0.1 eV/atom (~ 1200 K). Phonon calculations in the $P2_1/m$ phase revealed imaginary frequencies. By following the most unstable of the modes at the Γ point (see Figure. 4(c)), we successfully obtained the basic phase $P\bar{3}$ FeSi_2O_6 .

In short, both binary end members, $Pnma$ FeO_2 and Fe_2P -type SiO_2 , with proper ionic substitutions and subsequent displacement/relaxation, can produce the basic $P\bar{3}$ -type FeSi_2O_6 phase. This means the latter can be viewed as a straightforward pseudo-binary of the FeO_2 and SiO_2 end members. This exercise also shows that the $Pnma$ -type FeO_2 structure and Fe_2P -type and cotunnite-type SiO_2 structures are closely related.

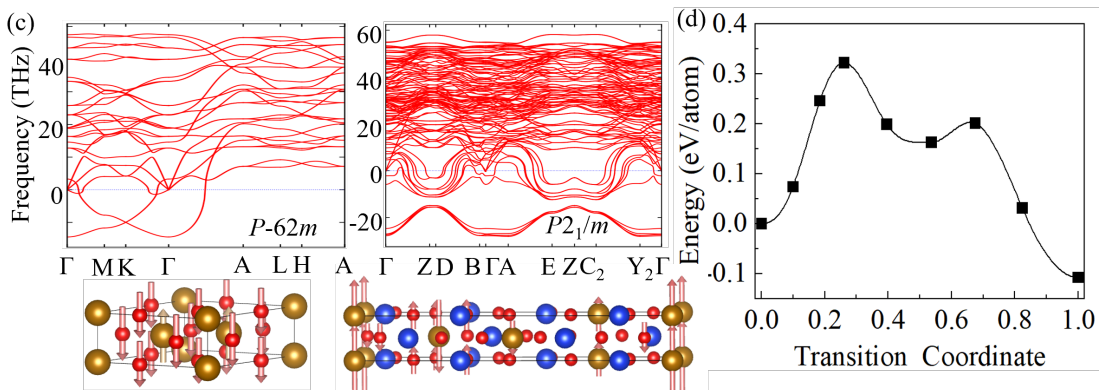
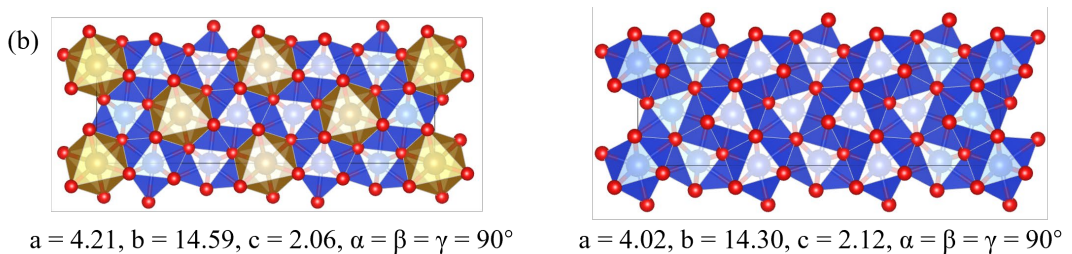
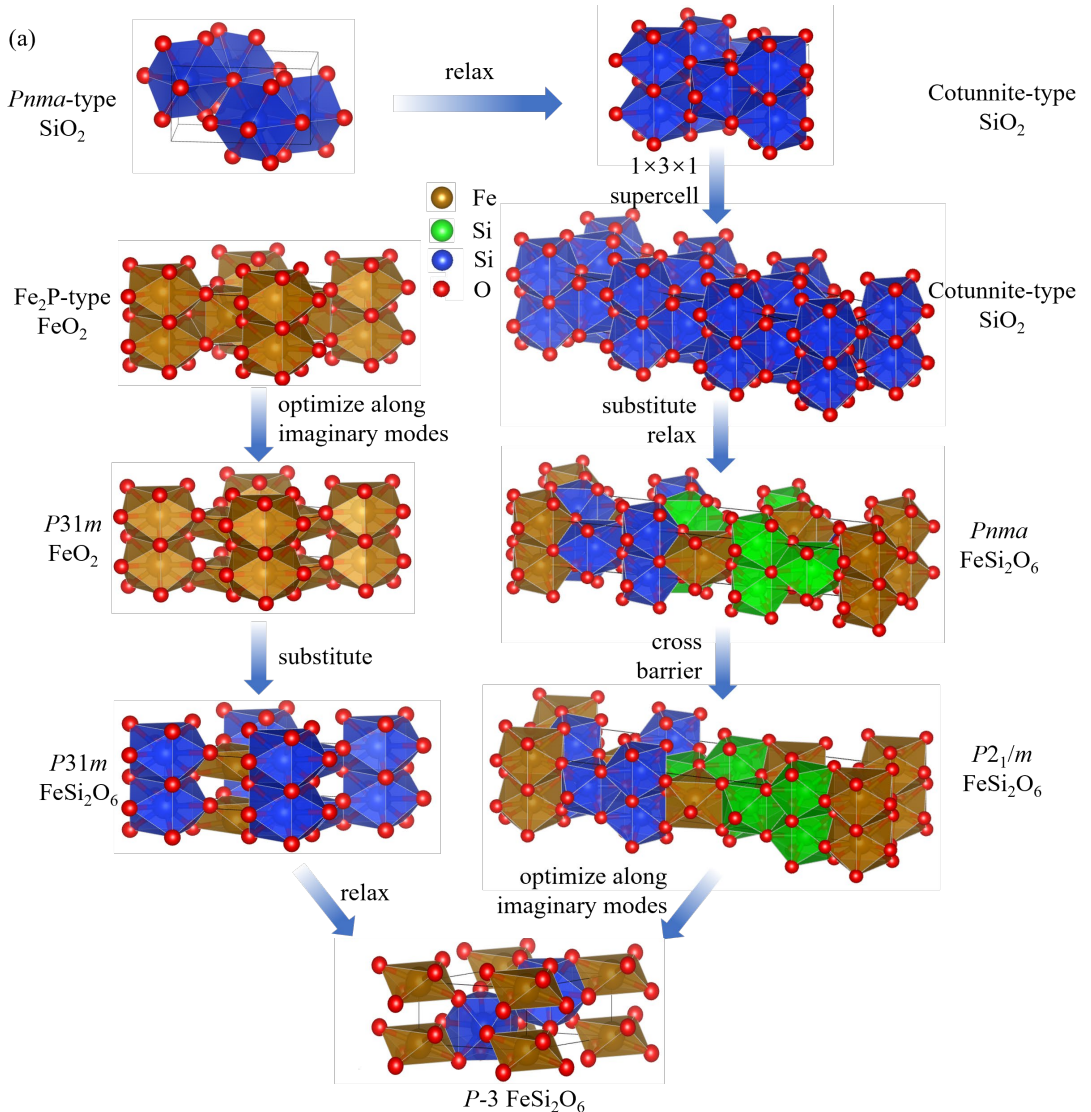


Figure 4. (a) Two pathways from Fe₂P-type FeO₂ and *Pnma*-type SiO₂ at 1 TPa to $P\bar{3}$ FeSi₂O₆. (b) Three-fold cotunnite-type SiO₂ supercell and four-fold orthorhombic FeSi₂O₆ supercell. (c) The phonon dispersion of Fe₂P-type (*P*-62*m*) FeO₂ and *P*2₁/*m* FeSi₂O₆. The arrows on the atoms denote the directions of the selected unstable mode at the Γ point. (d) NEB calculation of the energy barrier for the *Pnma* to *P*2₁/*m* transition in FeSi₂O₆. The green Si atoms shown in (a) are required to be displaced along the *c*-axis.

3.4 Energetics under Pressure and Increased Temperature

To investigate the high-temperature stability of these phases, we computed the Gibbs free energy of all phases involved and the phase diagram for the FeO₂-SiO₂ pseudo-binary system at 1 TPa. As depicted in Figure. 5(a), with increasing temperature, the *P*3 FeSiO₄ and *P*3 Fe₄Si₅O₁₈ phases transition from stable to metastable states. Conversely, $P\bar{3}$ FeSi₂O₆ emerges as the sole stable phase within the pseudo-binary system above 4000 K. Figure. 5(b) shows free energies excluding vibrational contributions. The inclusion of vibrational contributions further stabilizes all three ternary phases relative to their binary end members. The considerably larger density of states at the Fermi level in $P\bar{3}$ FeSi₂O₆ makes the electronic entropy a major stabilization factor for this phase at high temperatures (see Figure. S2).

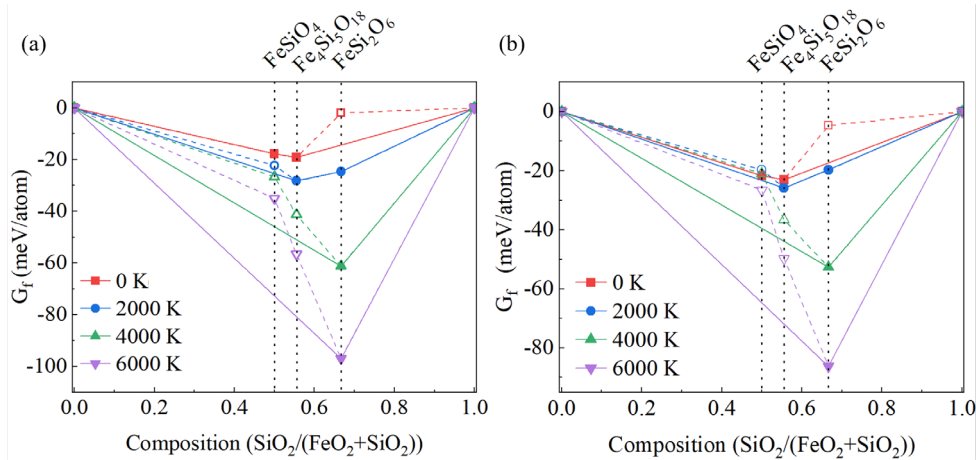


Figure 5. (a) Gibbs free energies with increasing temperature, including vibrational and electronic excitation contributions at 1 TPa. (b) Free energies including only thermal electronic excitation. Free energies are plotted relative to the ground state phases of FeO₂ and SiO₂ at various temperatures.

Solid markers represent convex hull points, while open ones indicate metastable structures.

We evaluated the stability fields of the three phases discovered in the Fe-Si-O system for three Fe/Si ratios: 1.0, 0.8, and 0.5, as in the three phases identified. Figure. 6 presents the pressure-temperature conditions at the core-mantle boundary (CMB) of super-Earths [2] with various Earth masses (M_{\oplus}). And it shows that the Fe-Si-O system exhibits complex phase transitions within the temperature and pressure ranges investigated in our study. The relevant phase transitions in FeO , FeO_2 , and SiO_2 are shown in Figure. S3.

For $\text{Fe/Si} = 1.0$, FeSiO_4 is stable in terrestrial mantles of super-Earths with up to $\sim 4.5M_{\oplus}$. For planets with masses larger than $\sim 4.5M_{\oplus}$, FeSiO_4 dissociates into FeSi_2O_6 and FeO_2 (see Figure. 6(a)). For $1/2 < \text{Fe/Si} < 1$, e.g., 4/5, FeSiO_4 and SiO_2 coexist for masses below $\sim 3.5M_{\oplus}$. Between ~ 3.5 and $\sim 4.5M_{\oplus}$ the system undergoes a recombination transition in which FeSiO_4 plus FeSi_2O_6 co-exist, whereas for masses in excess of $\sim 4.5M_{\oplus}$ FeSi_2O_6 and FeO_2 are stable phases (see Figure. 6(b)). For $\text{Fe/Si} \leq 1/2$, FeSiO_4 plus SiO_2 are stable for masses up to $\sim 3.5M_{\oplus}$, while FeSi_2O_6 stabilizes in mantles of planets with masses above $\sim 3.5M_{\oplus}$ (see Figure. 6(c)).

Under super-Earth CMB conditions, with increasing depth, the fate of $P3$ FeSiO_4 is controlled by the local SiO_2 budget, and we summarized the Clapeyron Slopes (CS) for each transition stage. In SiO_2 -deficient environments ($\text{Fe/Si} = 1$), the complete dissociation of FeSiO_4 into FeSi_2O_6 and FeO_2 will occur ($\text{CS} = -109.9 \text{ MPa/K}$); when SiO_2 is slightly in excess ($\text{Fe/Si} = 4/5$), FeSiO_4 efficiently scavenges the available SiO_2 to form FeSi_2O_6 ($\text{CS} = -72.2 \text{ MPa/K}$), while any residual FeSiO_4 is subsequently converted to FeSi_2O_6 plus FeO_2 ($\text{CS} = -109.9 \text{ MPa/K}$); in SiO_2 -rich regimes ($\text{Fe/Si} = 1/2$), all FeSiO_4 can recombine with SiO_2 and be completely transformed into FeSi_2O_6 ($\text{CS} = -72.2 \text{ MPa/K}$). These Clapeyron Slopes are unusually large compared to phase transitions in the Earth's mantle.

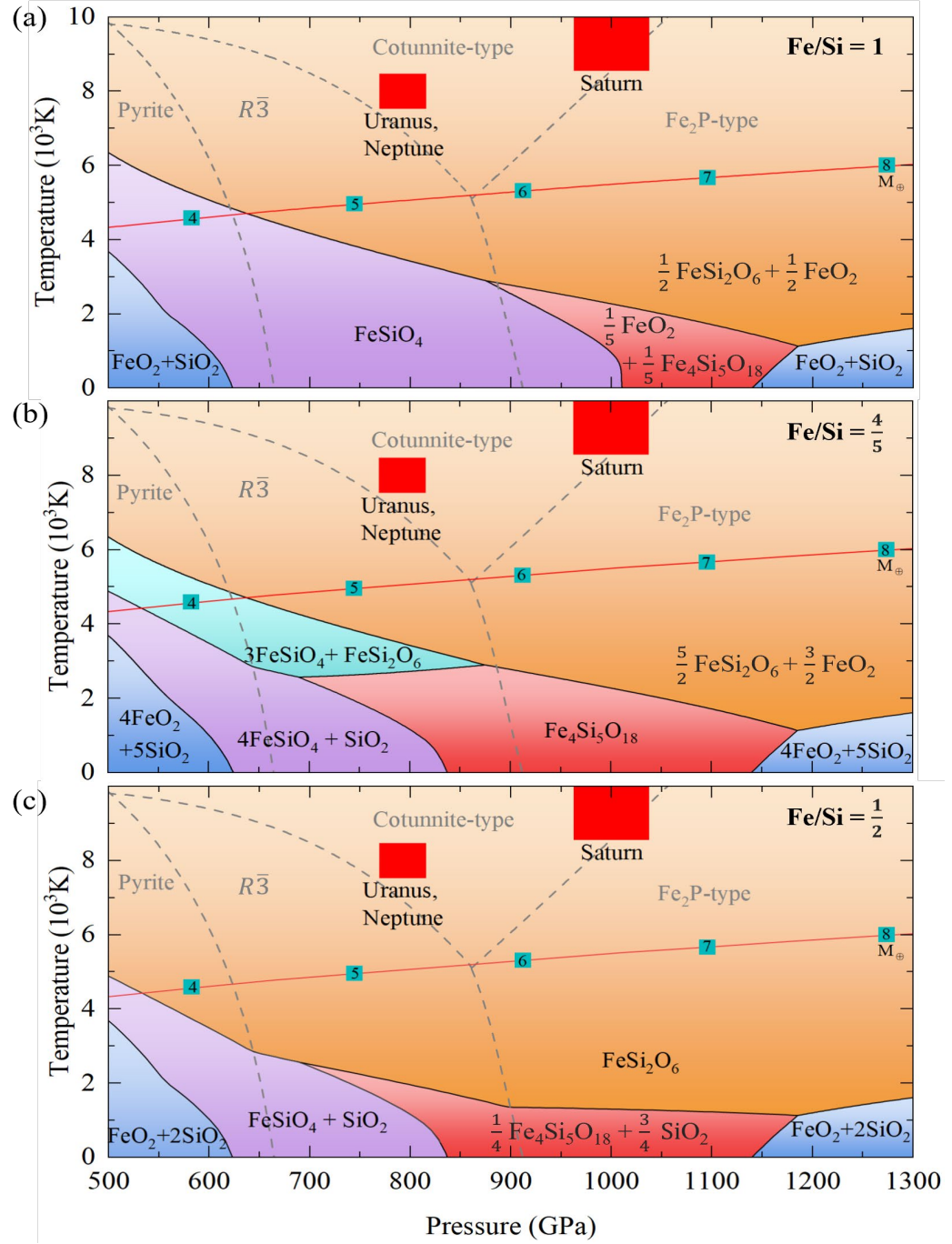


Figure 6. Phase diagram of the three new phases: (a) $P3\ FeSiO_4$, (b) $P3\ Fe_4Si_5O_{18}$, and (c) $P\bar{3}\ FeSi_2O_6$. The red line and small blue squares show the CMB pressure-temperature conditions for super-Earths [2]. Associated numbers refer to the planet mass expressed in Earth-mass units (M_\oplus). Red squares mark Guillot's estimated CMB pressure-temperature conditions for the solar giants [46]. The gray dashed lines mark the phase boundaries of SiO_2 .

Summary and conclusions

We systematically investigated high-pressure phase relations in the Fe-Si-O system

at ~ 1 TPa using the AGA method combined with *ab initio* LDA calculations. Two stoichiometric compounds, $P3$ FeSiO_4 and $P3$ $\text{Fe}_4\text{Si}_5\text{O}_{18}$, were found to be stable at 0K, while $P\bar{3}$ FeSi_2O_6 was shown to stabilize at high temperatures. These compounds exhibit similar structural building blocks (polyhedral) and can be viewed as $\text{FeO}_2\text{-SiO}_2$ pseudo-binary phases characterized as metallic, paramagnetic systems. The crystal structure of $P\bar{3}$ FeSi_2O_6 can be obtained by replacing Si by Fe in Fe_2P -type SiO_2 or Fe by Si in *Pnma* FeO_2 , the stable elementary oxides at 1 TPa. $P3$ FeSiO_4 and $P3$ $\text{Fe}_4\text{Si}_5\text{O}_{18}$ can be readily obtained by substituting the appropriate Si by Fe in $P\bar{3}$ FeSi_2O_6 .

In the Earth's silicate mantle, Fe^{+2} enters as $[\text{Fe}]_{\text{Mg}}$ in Mg-silicate phases, e.g., $(\text{Mg},\text{Fe})\text{SiO}_3$ bridgmanite and $(\text{Mg},\text{Fe})_2\text{SiO}_4$ olivine. Fe^{+3} can enter as a coupled substitution $[2\text{Fe}]_{\text{Mg},\text{Si}}$, e.g., $(\text{Mg},\text{Fe})(\text{Si},\text{Fe})\text{O}_3$ in bridgmanite, but usually, aluminum is favored on the silicon site ($[\text{Al}]_{\text{Si}}$) [47]. By analogy, Fe is also thought to "dissolve" mainly as $[\text{Fe}]_{\text{Mg}}$ or $[2\text{Fe}]_{\text{Mg},\text{Si}}$ in the canonical TPa silicate hosts, i.e., $I\bar{4}2d$ -type Mg_2SiO_4 or $P2_1/c$ -type MgSi_2O_5 . Prior to this work, no stable Fe-Si-O compounds have ever been reported at TPa pressures. Our discovery of the $(\text{Fe},\text{Si})\text{O}_2$ pseudo-binary phases may not necessarily alter the phase transition sequence of the Mg-Si-O system if Fe is present in low concentrations. It is certain, however, that small amounts of Fe will open two-phase fields (binary loops) in the Mg-Si-O phase diagram [1].

Our new $\text{FeO}_2\text{-SiO}_2$ pseudo-binary phases show that Fe favors an FeO_2 -type component over the FeO one and possibly $[\text{Fe}]_{\text{Si}}$ substitution over $[\text{Fe}]_{\text{Mg}}$ at TPa pressures. Mg/Si disorder in $I\bar{4}2d$ -type Mg_2SiO_4 might change this intuitive notion, and a careful study of Mg/Si/Fe disorder in this system needs to be carried out. One can anticipate that the abundance of the FeO_2 component, which in the deep Earth's mantle can be produced by dehydrogenation of goethite FeOOH [48], will be a determining factor in the formation of the pseudo-binaries and on the solubility of Fe in the canonical silicates and their abundances at TPa pressures.

In short, the existence of our newly discovered $\text{FeO}_2\text{-SiO}_2$ pseudo-binaries implies a markedly different pattern of Fe incorporation into high-pressure Mg-silicates at TPa

conditions, compared with the behavior inferred at the GPa pressures of Earth's mantle.

Acknowledgments

This research was supported by the National Natural Science Foundation of China (Nos. 12374015, T2422016, and 42374108). Shaorong Fang and Tianfu Wu from the Information and Network Center at Xiamen University are acknowledged for their assistance with Graphics Processing Unit (GPU) computing. The work at Columbia University was supported by the Gordon and Betty Moore Foundation Award GBMF12801 42 (doi.org/10.37807/GBMF12801) and results from a collaboration established under NSF Grants EAR-2000850 and EAR-1918126.

References

- [1] K. Umemoto, R. M. Wentzcovitch, S.Q. Wu et al., Phase transitions in MgSiO₃ post-perovskite in super-Earth mantles. *Earth Planet. Sci. Lett.* 478, 40-45 (2017).
- [2] A. P. van den Berg, K. Umemoto, D. Yuen, R. M. Wentzcovitch, Mass-dependent dynamics of terrestrial exoplanets using ab initio mineral properties. *Icarus* 317, 412-426 (2019).
- [3] J. J. Fortney, M. S. Marley, and J. W. Barnes, Planetary Radii across Five Orders of Magnitude in Mass and Stellar Insolation: Application to Transits. *Astrophys. J.* 659 1661 (2007).
- [4] S. Seager, M. Kuchner, C. A. Hier-Majumder et al., Mass-Radius Relationships for Solid Exoplanets. *Astrophys. J.* 669 1279 (2007).
- [5] M. Murakami, K. Hirose, K. Kawamura, N. Sata, Y. Ohishi, Post-Perovskite Phase Transition in MgSiO₃. *Science* 304, 855-858 (2004).
- [6] T. Tsuchiya, J. Tsuchiya, K. Umemoto, R. M. Wentzcovitch, Phase transition in MgSiO₃ perovskite in the Earth's lower mantle, *Earth Planet. Sci. Lett.* 224, 241-248 (2004).
- [7] A. R. Oganov, S. Ono, Theoretical and experimental evidence for a post-perovskite phase of MgSiO₃ in Earth's D'' layer. *Nature* 430, 445-448 (2004).
- [8] B. E. McArthur, M. Endl, W. D. Cochran et al., Detection of a Neptune-Mass

- Planet in the ρ^1 Cancri System Using the Hobby-Eberly Telescope. *Astrophys. J.* 614 L81 (2004).
- [9] K. Umemoto, R. M. Wentzcovitch, and P. B. Allen, Dissociation of MgSiO_3 in the Cores of Gas Giants and Terrestrial Exoplanets. *Science* 311, 983-986 (2006).
- [10] K. Umemoto, R. M. Wentzcovitch, Two-stage dissociation in MgSiO_3 post-perovskite. *Earth Planet. Sci. Lett.* 311, 225–229 (2011).
- [11] H. Niu, A. R. Oganov, X. Q. Chen D. Li, Prediction of novel stable compounds in the Mg-Si-O system under exoplanet pressures. *Sci Rep* 5, 18347 (2016).
- [12] S. Wu, K. Umemoto, R. M. Wentzcovitch et al., Identification of post-pyrite phase transitions in SiO_2 by a genetic algorithm. *Physical Review B* 83: 184102 (2011).
- [13] T. Tsuchiya, J. Tsuchiya, Prediction of a hexagonal SiO_2 phase affecting stabilities of MgSiO_3 and CaSiO_3 at multimegarbar pressures. *Proc. Natl. Acad. Sci. U.S.A.* 108, 1252 (2011).
- [14] C. Liu et al., Mixed Coordination Silica at Megabar Pressure. *Phys Rev Lett.* Jan 22;126(3):035701. (2021).
- [15] K. Umemoto, and R. M. Wentzcovitch, Ab initio exploration of post-PPV transitions in low-pressure analogs of MgSiO_3 . *Phys. Rev. Materials* 3, 123601 (2019).
- [16] K. Umemoto, and R. M. Wentzcovitch, Ab initio prediction of an order-disorder transition in Mg_2GeO_4 : Implication for the nature of super-Earth's mantles. *Phys. Rev. Materials* 5, 093604 (2021).
- [17] B. Grocholski, S. -H. Shim, V. B. Prakapenka, Stability of the MgSiO_3 analog NaMgF_3 and its implication for mantle structure in super-Earths. *Geophys. Res. Lett.* 37, L14204 (2010).
- [18] R. Dutta, E. Greenberg, V. B. Prakapenka et al., Phase Transitions beyond post-perovskite in NaMgF_3 to 160 GPa. *Proc. Nat. Acad. Sci.* 116, 19324-19329 (2019).
- [19] R. Dutta, S. J. Tracy, R. E. Cohen et al., Ultrahigh-pressure disordered eight-coordinated phase of Mg_2GeO_4 : Analogue for super-Earth mantles, *Proc. Natl. Acad. Sci. U.S.A.* 119 (8) e2114424119 (2022).
- [20] R. Dutta, S. J. Tracy, and R. E. Cohen, High-pressure order-disorder transition in

- Mg_2SiO_4 : Implications for super-Earth mineralogy. Phys. Rev. B 107,184112 (2023).
- [21] G. L. Weerasinghe et al., Computational searches for iron oxides at high pressure. J. Phys.: Condens. Matter 27 455501 (2015).
- [22] F. Zheng et al., Structure and motifs of iron oxides from 1 to 3 TPa. Phys. Rev. Materials 6, 043602 (2022).
- [23] S. Wu et al., An adaptive genetic algorithm for crystal structure prediction. J. Phys.: Condens. Matter 26 035402 (2014).
- [24] N. D. Mermin, Thermal Properties of the Inhomogeneous Electron Gas, Phys. Rev. 137, A1441 (1965).
- [25] R. M. Wentzcovitch, J. L. Martins, and P. B. Allen, Energy versus free-energy conservation in first-principles molecular dynamics. Phys. Rev. B 45, 11372 (1992)
- [26] P. Giannozzi et al., QUANTUM ESPRESSO: a modular and open-source software project for quantum simulations of materials. J Phys-Condens Mat 21 (2009).
- [27] P. Giannozzi et al., Advanced capabilities for materials modelling with QUANTUM ESPRESSO. J Phys-Condens Mat. 29 (2017).
- [28] D. Vanderbilt, Soft self-consistent pseudopotentials in a generalized eigenvalue formalism. Phys. Rev. B 41, 7892 (1990).
- [29] K. Umemoto, R. M. Wentzcovitch, Y. G. Yu, R. Requist, Spin transition in $(\text{Mg},\text{Fe})\text{SiO}_3$ perovskite under pressure. Earth Planet. Sci. Lett. 276, 198 (2008).
- [30] C. G. Broyden, The Convergence of a Class of Double-rank Minimization Algorithms 2. The New Algorithm. IMA J. Appl. Math. 6, 222 (1970)..
- [31] R. Fletcher, A new approach to variable metric algorithms. Comput. J. 13, 317 (1970).
- [32] D. Goldfarb, A family of variable-metric methods derived by variational means. Math. Comput. 24, 23 (1970).
- [33] D. F. Shanno, An example of numerical nonconvergence of a variable-metric method. Math. Comput. 24, 647 (1970).
- [34] A. Togo, I. Tanaka, First principles phonon calculations in materials science. Scripta Mater. 108, 1 (2015).

- [35] D. C. Wallace, H. Callen, Thermodynamics of crystals. *Am. J. Phys.* 40, 1718–1719 (1972).
- [36] J. D. Althoff, P. B. Allen, and R. M. Wentzcovitch and J. A. Moriarty, Phase diagram and thermodynamic properties of solid magnesium in the quasiharmonic approximation. *Phys. Rev. B* 48, 13253 (1993).
- [37] T. Qin, Q. Zhang, R. M. Wentzcovitch and K. Umemoto, qha: A Python package for quasiharmonic free energy calculation for multi-configuration systems. *Comput. Phys. Commun.* 237, 199 (2019).
- [38] S. M. Foiles, M. I. Baskes and M. S. Daw, Embedded-atom-method functions for the fcc metals Cu, Ag, Au, Ni, Pd, Pt, and their alloys. *Phys. Rev. B* 33, 7983 (1986).
- [39] A. Banerjea, J. R. Smith, Origins of the universal binding-energy relation, *Phys. Rev. B* 37, 6632 (1988).
- [40] P. Brommer, F. Gähler, Effective potentials for quasicrystals from ab-initio data. *Philos. Mag.* 86, 753 (2006).
- [41] P. Brommer and F. Gähler, Potfit: effective potentials from ab initio data. *Modell. Simul. Mater. Sci. Eng.* 15, 295 (2007).
- [42] A. Grzechnik, K. Friese, Crystal structures and stability of NaLnF₄ (Ln = La, Ce, Pr, Nd, Sm and Gd) studied with synchrotron single-crystal and powder diffraction. *Dalton Trans.* 41, 10258 (2012).
- [43] R. Shi, C. D. S. Brites and L. D. Carlos, Hexagonal-phase NaREF₄ upconversion nanocrystals: the matter of crystal structure. *Nanoscale* 13, 19771 (2021).
- [44] X. Mao, J. A. Dawson, Optimizing Li-Ion Transport in LaCl_{3-x}Br_x solid electrolytes through anion mixing. *EcoMat* 7, e70006(2025).
- [45] G. Henkelman, H. Jónsson, Improved tangent estimate in the nudged elastic band method for finding minimum energy paths and saddle points. *J. Chem. Phys.* 113, 9978–9985 (2000).
- [46] T. Guillot, Special issue: Probing the giant planets, *Phys. Today* 57, No. 4, 63 (2004).
- [47] H. Hsu, Y. G. Yu and R. M. Wentzcovitch, Spin crossover of iron in aluminous

MgSiO₃ perovskite and post-perovskite. *Earth Planet. Sci. Lett.* 359, 34–39 (2012).
[48] Q. Hu, D. Y. Kim, H. Mao et al. FeO₂ and FeOOH under deep lower-mantle
conditions and Earth's oxygen–hydrogen cycles. *Nature* 534, 241–244 (2016).